

# Inferring fission timescales from precission neutron multiplicity using a Langevin dynamical model

G. Mohanto <sup>1,2</sup>, M. T. Senthil Kannan,<sup>3</sup> Jhilmam Sadhukhan <sup>3,2,\*</sup> and B. Srinivasan<sup>1,†</sup>

<sup>1</sup>*Nuclear Physics Division, Bhabha Atomic Research Centre, Mumbai 400085, India*

<sup>2</sup>*Homi Bhabha National Institute, Training School Complex, Anushaktinagar, Mumbai 400094, Maharashtra, India*

<sup>3</sup>*Physics Group, Variable Energy Cyclotron Centre, 1/AF-Bidhannagar, Kolkata 700064, India*



(Received 27 July 2023; revised 14 July 2024; accepted 13 August 2024; published 6 September 2024)

**Background:** In the theoretical analysis of nuclear fission observables, dissipation strength is often adjusted locally to reproduce the experimental data. The global trend of the dissipation strength over the whole mass range of fissioning nuclei is still not known convincingly. Also, its connection with fission timescales is essential to understand the reaction dynamics.

**Purpose:** We extracted the nuclear dissipation strength by reproducing the experimental precission neutron multiplicities for reactions forming compound nuclei in the mass range of  $168 \leq A \leq 256$ . Subsequently, we predicted the systematics of fission lifetime over this range of compound nuclear mass.

**Method:** We employed a one-dimensional Langevin dynamical model for fission, where shape-dependent shell correction and one-body dissipation are used. The dissipation strengths for different compound systems are extracted by reproducing the measured precission neutron multiplicities. Obtained strengths are shown to consistently reproduce the average total kinetic energy of the fission fragments. Subsequently, dynamical fission-time distributions were simulated in coincidence with these neutron multiplicities.

**Results:** We identified three different mass regions depending on the required dissipation strength: (i) for compound nuclear mass number  $A < 210$ , the role of dissipation is minimal, (ii) in  $210 \lesssim A \lesssim 244$ , shell correction is found to influence the dissipation strength strongly, and (iii) for  $A \gtrsim 244$  the dynamics is strongly driven by dissipation. Further, for lighter masses with a fission barrier height between 18 and 30 MeV, fission time appeared to depend very weakly on the fission barrier, whereas, for heavy nuclei, fission time is shown to be well correlated with the barrier height of the primary compound nucleus.

**Conclusion:** Our paper provides a global understanding of the nuclear dissipation strength and the fission lifetime based on the experimental neutron multiplicities. These systematics will be helpful in estimating fission time in heavy ion-induced reactions.

DOI: [10.1103/PhysRevC.110.034604](https://doi.org/10.1103/PhysRevC.110.034604)

## I. INTRODUCTION

Nuclear fission provides an ideal platform to investigate the large amplitude collective dynamics in a strongly interacting many-body system. However, it involves tremendous intricacies originating from the nontrivial nature of the inter-nucleonic interactions. Consequently, although the dissipation of collective energy in nuclear collective dynamics is well established [1], a systematic global understanding of such a dissipative phenomenon over the whole range of fissioning nuclei is yet to be explored comprehensively within a dynamical framework. Especially understanding the characteristics of nuclear dissipation is still an open field of research [2–6]. In the present-day scenario, the classical shape-dependent one-body dissipation mechanism is the best available tool to represent nuclear dissipation at low excitation energies [7–11]. However, a constant shape-independent dissipation strength is often used as a free parameter in

theoretical analysis [12–14]. It is usually adjusted locally for a certain limited number of compound nuclei (CN) in order to analyze different experimental probes like neutron multiplicities [15–17], evaporation residue (ER) cross sections [18,19], charged particle multiplicities [20], and fragment yields [21,22]. Particularly, even with the intrinsic shape dependence, a single prescription of the dissipation strength cannot reproduce the experimental data of a specific probe (for example, either precission neutron multiplicity or ER cross section) in the whole mass range of  $150 \lesssim A \lesssim 250$ .

Average precission neutron multiplicity ( $\nu_{\text{pre}}$ ) is an important probe frequently used to gauge the dissipation strength. Within the concept of *neutron clock*, it is assumed that the average fission time ( $\langle t_f \rangle$ ) can be inferred from  $\nu_{\text{pre}}$  as  $\langle t_f \rangle = \nu_{\text{pre}} \tau_n$  [23], where  $\tau_n$  is the average decay time for neutron evaporation. In practice,  $\tau_n$  is calculated for each successive decay channel by employing the standard statistical model [24] and  $\langle t_f \rangle$  is estimated by reproducing the experimental  $\nu_{\text{pre}}$  within the statistical model for fission [25], where the dissipation strength controls fission decay width. However, it has been shown [26] that the actual fission time, when the compound nucleus bifurcates into two fragments,

\*Contact author: jhilams@gmail.com

†Contact author: bsrini15@gmail.com

may be larger than the fission time predicted by the neutron clock technique. Therefore, the connection between  $\nu_{\text{pre}}$  and  $\langle t_f \rangle$  is not straightforward. An appropriate dynamical model needs to be implemented to correlate these two quantities. In this process, nuclear dissipation plays an important role. Moreover, the variation of dissipation strength with deformation is also crucial to deciding  $\nu_{\text{pre}}$  and the fission timescale.

In different works, statistical model analysis has been performed [12,27,28] to determine the dissipation strength over different mass regions by comparing the experimental  $\nu_{\text{pre}}$ , ER, and fission cross sections. However, several realistic considerations are beyond the scope of such statistical model estimations. A few of them are the following: (i) shape dependencies in the input variables cannot be incorporated, (ii) dynamical time evolution during the saddle-to-scission transition is either approximated or completely neglected, and (iii) actual scission time at the point of bifurcation of the compound nucleus cannot be determined accurately.

In the present paper, we have studied  $\nu_{\text{pre}}$  to extract a global trend of nuclear dissipation within the wall-plus-window model [29] of one-body dissipation. We have performed stochastic Langevin dynamical calculations for fissioning nuclei covering the compound nuclear mass range of  $168 \leq A \leq 256$ . Further, we extracted the fission lifetime for all these nuclei from our dynamical model to infer the correlation between fission lifetime and other input quantities. The theoretical formalism is discussed in Sec. II. Then, Sec. III describes the results, and we finally conclude in Sec. IV.

## II. THEORETICAL FORMALISM

We simulate the collective evolution of nuclei along the elongation/fission degree of freedom, which is defined with the help of the funny hill [30] parameter  $c$ . In general, the neck parameter  $h$  and mass asymmetry  $\alpha$  along with  $c$  define a fissioning shape more accurately while exploring the fission-fragment properties. However, both of these parameters are close to zero [31,32] around the ground state configuration, where the majority of the neutrons are evaporated [33]. Further, the significance of  $\alpha$  reduces as excitation energy increases. Therefore, for the present purpose, we restrict our calculations to  $h = 0$  and  $\alpha = 0$ . It substantially enhances the numerical efficiency. The time propagation of  $c$  is followed with the stochastic Langevin equation [1,26,34,35]:

$$\begin{aligned} \frac{dp}{dt} &= -\frac{p^2}{2} \frac{d}{dc} \left( \frac{1}{\mathcal{M}(c)} \right) - \frac{dF}{dc} - \eta(c)p + g(c)\Gamma(t), \\ \frac{dc}{dt} &= \frac{p}{\mathcal{M}(c)}, \end{aligned} \quad (1)$$

where  $p$  is the momentum conjugate to  $c$  and  $\mathcal{M}(c)$  represents the shape-dependent collective inertia. The Werner-Wheeler approximation [36] for the irrotational flow of incompressible nuclear fluid is used to determine  $\mathcal{M}(c)$ . The one-body dissipation mechanism is considered to estimate the shape-dependent dissipation coefficient  $\eta(c)$  [32]. The term  $g(c)$  in Eq. (1) represents the strength of the random force, and  $\Gamma(t)$  is its time-dependent part following the time correlation properties:  $\langle \Gamma(t) \rangle = 0$  and  $\langle \Gamma(t_1)\Gamma(t_2) \rangle = \delta(t_1 - t_2)$ . Also,

TABLE I. Details of reactions used in the present paper. Fission barriers  $V_B^{\text{LD}}$  and  $V_B$  are in MeV.

S. no.	CN	Reaction	$V_B^{\text{LD}}$	$V_B$	Ref.
1	$^{168}\text{Yb}$	$^{18}\text{O} + ^{150}\text{Sm}$	25.61	27.00	[44]
2	$^{178}\text{W}$	$^{19}\text{F} + ^{159}\text{Tb}$	21.05	21.78	[44]
3	$^{200}\text{Pb}$	$^{19}\text{F} + ^{181}\text{Ta}$	12.28	18.52	[44]
4	$^{204}\text{Pb}$	$^{18}\text{O} + ^{186}\text{W}$	12.93	22.23	[45]
5	$^{206}\text{Po}$	$^{12}\text{C} + ^{194}\text{Pt}$	10.40	19.0	[46]
6	$^{210}\text{Po}$	$^{18}\text{O} + ^{192}\text{Os}$	10.95	22.92	[44]
7	$^{210}\text{Rn}$	$^{16}\text{O} + ^{194}\text{Pt}$	8.40	17.98	[44]
8	$^{212}\text{Rn}$	$^{18}\text{O} + ^{194}\text{Pt}$	8.70	19.81	[44]
9	$^{213}\text{Fr}$	$^{16}\text{O} + ^{197}\text{Au}$	7.66	18.46	[44]
10	$^{216}\text{Ra}$	$^{12}\text{C} + ^{204}\text{Pb}$	6.94	15.21	[47]
11	$^{239}\text{Np}$	$^1\text{H} + ^{238}\text{U}$	4.46	7.75	[48]
12	$^{243}\text{Am}$	$^{11}\text{B} + ^{232}\text{Th}$	3.42	7.51	[49]
13	$^{244}\text{Cm}$	$^{12}\text{C} + ^{232}\text{Th}$	2.93	6.63	[49]
14	$^{248}\text{Cf}$	$^{16}\text{O} + ^{232}\text{Th}$	2.14	7.07	[49]
15	$^{251}\text{Es}$	$^{19}\text{F} + ^{232}\text{Th}$	1.84	7.94	[44]
16	$^{254}\text{Fm}$	$^{16}\text{O} + ^{238}\text{U}$	1.57	7.75	[23,50]
17	$^{256}\text{Fm}$	$^{18}\text{O} + ^{238}\text{U}$	1.61	7.35	[23]

$g(c)$  is related to  $\eta(c)$  by Einstein's fluctuation-dissipation theorem:  $g(c) = \sqrt{\eta(c)T}$ . Nuclear temperature  $T$  is calculated from the ground state excitation energy  $E^*$  and the ground state level density parameter  $a_0$  by using the Fermi gas expression:  $T = \sqrt{E^*/a_0}$ . Although the excitation energy changes with deformation,  $T$  is determined at the ground state configuration and kept constant along  $c$  as demanded by canonical thermodynamics. The driving potential for the collective dynamics is obtained from the Helmholtz free energy [37],  $F(c, T) = V(c) - [a(c, E^*) - a_0]T^2$ ,  $V(c)$  being the shell-corrected potential energy [26], and  $a(c, E^*)$  is the level density parameter as a function of  $c$  and  $E^*$ . The smooth liquid-drop part of  $V(c)$  is calculated from the double folding Yukawa-plus-exponential mean-field interaction [38]. The deformation-dependent shell correction energy in  $V(c)$  is calculated by employing the Strutinsky prescription [30,39], where the single-particle energies are computed from the Woods-Saxon mean field [40] with nuclear deformation defined from  $c$ . Also, the single-particle energies are corrected for the short-range pairing interaction, which is implemented within the well-known BCS scheme [39,40]. We have verified that the calculated fission barriers [ $V(c)$ ] of the chosen compound nuclei are consistent with previous calculations [41,42] from different models. Precisely, except for reactions 8, 9, 16, and 17 in Table I, deviation in the barrier height is  $<9\%$  from that predicted in [41], and it is further reduced in  $F$  due to high excitation energy.

We calculate  $a(c, E^*)$  from Ignatyuk's prescription [42]:

$$a(c, E^*) = \tilde{a}(c) \left( 1 + \frac{1 - \exp(-E^*/E_D)}{E^*} \delta E \right), \quad (2)$$

where  $E_D$  (18.5 MeV) and  $\delta E$  represent the shell damping rate with increasing  $E^*$  and the ground state shell correction energy for individual nuclei, respectively. The asymptotic value

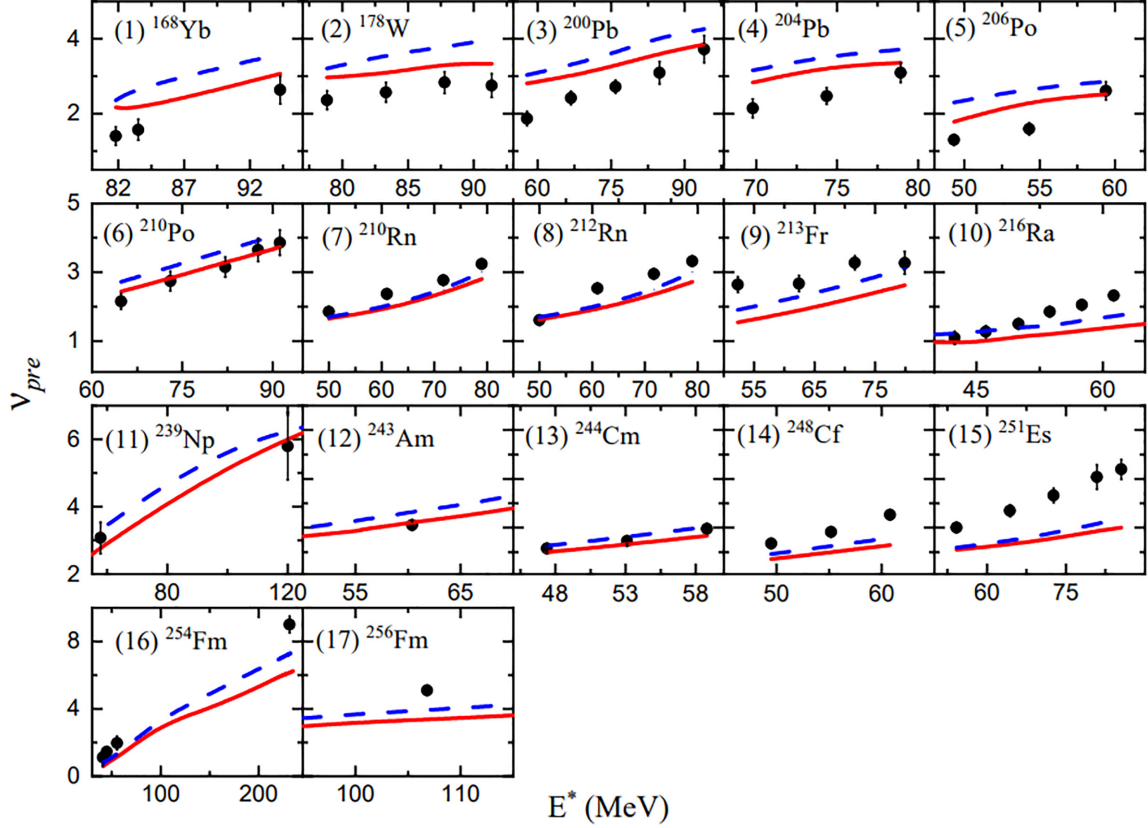


FIG. 1. The  $v_{pre}$ s calculated with CWWF (dashed lines) and  $WF^{0.25}$  (solid lines) are compared with measured data (symbols) for the reactions in Table I.

$\tilde{a}(c)$  is computed from the Reisdorf formula [43]:

$$\tilde{a}(c) = 0.04543r_0^3A + 0.1355r_0^2A^{\frac{2}{3}}B_s(c) + 0.1426r_0A^{\frac{1}{3}}B_k(c). \quad (3)$$

Here,  $A$  is the mass number, and  $r_0$  (1.12 fm) is the nuclear radius parameter defined from the  $s$ -wave neutron resonance spacing [43].  $B_s(c)$  and  $B_k(c)$  are the ratios of the integrated surface area and curvature, respectively, with respect to that of a spherical shape. The explicit  $E^*$  dependence in  $a$  contradicts the expression for  $T$  defined above. However, higher-order corrections in  $T$  are neglected to preserve the simple form of  $F$  given above [26].

During the collective evolution, evaporation of light particles such as neutrons, protons,  $\alpha$  particles, and statistical  $\gamma$  rays is considered at each Langevin time step. The Monte Carlo random sampling technique [1] is used for this purpose. The partial decay widths for these evaporation channels are calculated within Weisskopf's statistical theory [1,24], where nuclear level densities are obtained from the Fermi gas model, as mentioned above. These level densities are further enhanced owing to the low-lying collective excitations in nuclei. Such collective enhancements are incorporated in the present paper by following the procedure as suggested in [27,28,51].

Langevin equations are solved numerically using the finite difference method [34]. We expand Eq. (1) up to the second order in a small time increment  $\delta t = 10^{-25}$  s. It ensures better numerical accuracy in the presence of the fluctuating force

$\Gamma(t)$ . Further, depending on the compound system, an ensemble of a large number of Langevin events ( $2 \times 10^4 - 5 \times 10^4$ ) is computed to minimize the numerical fluctuations. Each of the Langevin trajectories is traced up to a maximum dynamical time of  $10^{-15}$  s, which is large enough to decide the fate of a fission event. Hence, in contrast to the standard practice [1], we could avoid any coupling with the statistical approach at the end of the dynamical propagation. The initial angular momentum of the CN in each event is sampled from the corresponding fusion spin distribution following the parameterization given in [1].

To validate our model calculations, we further estimated the average total kinetic energy (TKE) of the fission fragments. The expression for average TKE can be written as [31]

$$\langle E_K \rangle = \Delta + \langle E_{sc} \rangle + V_{sc} - V_n, \quad (4)$$

where  $\Delta$  is the mass difference between the compound nucleus and the fission fragments,  $V_{sc}$  represents the potential energy at scission, and  $V_n$  denotes the part of the fragment's kinetic energy required to overcome the nuclear attraction between the nascent fragments. In a one-dimensional model, only the collective kinetic energy at scission ( $E_{sc}$ ) varies due to thermal fluctuations, and we need to take the average over an ensemble of events to evaluate  $\langle E_K \rangle$ . It is clear from Eq. (4) that  $\langle E_K \rangle$  is sensitive to the scission criterion. We assumed the scission configuration at a deformation where the neck radius

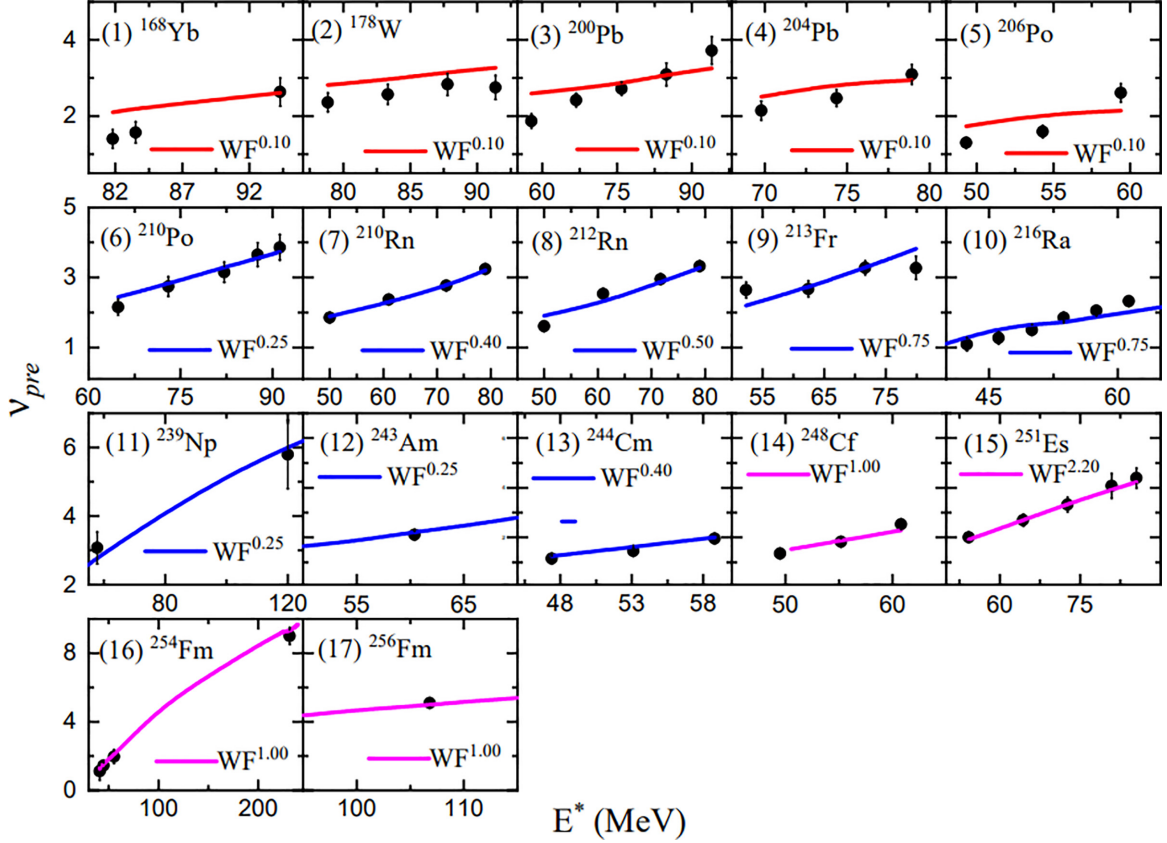


FIG. 2. The  $v_{pre}$ s calculated (solid lines) with the best-fit  $k_s$  (indicated in each panel) are compared with experimental data (symbols). The weak ( $k_s = 0.1$ ), moderate ( $0.25 \leq k_s \leq 1$ ), and strong ( $k_s \geq 1$ ) dissipations are indicated by red, blue, and magenta lines, respectively.

equals  $x_N R_0$  [30,36] with  $R_0 = r_0 A^{1/3}$  and  $x_N = 0.3$ . Although this condition has been shown to reproduce the measured  $\langle E_K \rangle$  for actinides correctly [36],  $x_N$  may differ for lighter compound nuclei.

### III. RESULT AND ANALYSIS

We selected reactions covering broad ranges of compound nuclear mass and excitation energy and excluded those reactions where entrance-channel effects are dominant [12]. The details of these reactions are listed in Table I where  $V_B^{LD}$  is the liquid drop barrier and  $V_B$  is the shell corrected barrier. The chosen actinide compound nuclei undergo asymmetric fission at low excitation energies, which is beyond the scope of a one-dimensional model. Therefore, for each of these reactions, we have carefully chosen the lowest excitation energy such that the relative contribution of the asymmetric mode with respect to the symmetric mode is negligible at and above this energy. We employed two different variants of one-body friction, namely the wall-plus-window friction (WF) [29] and the chaos-weighted wall-plus-window friction (CWCF) [52,53] for  $\eta(c)$  in Eq. (1).

The standard WF formula was derived by treating the collision of the nucleons of the moving wall classically and assuming that the nucleons would achieve complete equilibration before their succeeding collision with the surface.

However, quantum mechanics renders the collisions less than perfect, thereby weakening dissipation. Further, the nuclear shape may not be sufficiently irregular to produce complete equilibration. To account for all these effects, WF is often reduced by a constant scaling factor  $k_s$ .

In the rest of this paper, we denote this as  $WF^x$  for  $k_s = x$ . The value of  $k_s$  is often fixed at 0.25 [11,54–56] based on the fission data in the actinide region. However, the global trend of  $k_s$  over the different compound nuclear mass regions is still unknown. The CWCF, on the other hand, provides a more realistic alternative to the  $k_s$  factor, as nonchaotic behavior is properly taken care of in this prescription.

In Fig. 1, we compare our Langevin dynamical results on  $v_{pre}$ , for both  $WF^{0.25}$  and CWCF, with experimental data for the reactions in Table I. In this figure, the reactions are sorted according to the increasing mass of the CN. For all the reactions, CWCF predictions are higher than the  $WF^{0.25}$  calculations. In the case of  $A < 210$ , both  $WF^{0.25}$  and CWCF overpredict  $v_{pre}$ . For comparatively heavier CN with  $210 \leq A \lesssim 244$ , a better reproduction of the measured  $v_{pre}$  is observed except for the reactions 7–10 of Table I. For the rest of the reactions, i.e., for  $A > 244$ , both  $WF^{0.25}$  and CWCF underestimate the experimental  $v_{pre}$ . As shown in earlier works [11,53], CWCF performs better for heavy nuclei. Therefore, we generally see that, explaining all the reactions using a single model, either CWCF or  $WF^{0.25}$

is impossible. Since  $\nu_{\text{pre}}$  is related to the fission timescale, explaining the value of  $\nu_{\text{pre}}$  requires a more delicate adjustment of the dissipation strength  $\eta(c)$  that directly controls the compound nuclear fission time. To get a correct estimate of the fission timescale, we recalculate  $\nu_{\text{pre}}$  for all the reactions in Table I by using WF with  $k_s$  as a free parameter. We varied the value of  $k_s$  between 0.1 and 1.0 to fit the experimental data. Only for the reaction 15, a much higher  $k_s$  (2.2) is required. Calculated  $\nu_{\text{pre}}$  with the best-fit  $k_s$ s are shown in Fig. 2 along with the experimental data. We can now grossly differentiate the reactions into three categories based on the required  $k_s$  and the corresponding liquid-drop fission barrier  $V_B^{\text{LD}}$ . For reactions 1–5, the  $V_B^{\text{LD}}$  is too high, and the dynamics is primarily controlled by the driving potential  $F$  in Eq. (1). Hence,  $\nu_{\text{pre}}$ s are not quite sensitive to  $k_s$  and, as Fig. 2 shows,  $\text{WF}^{0.10}$  provides an upper limit to the required dissipation strength for these reactions. Secondly, for the midbarrier ( $3 \lesssim V_B^{\text{LD}} \lesssim 9$  MeV) systems (reactions 7–13), both the driving potential and the nuclear dissipation are important, and  $k_s$  varies between 0.25 and 0.75 depending on the detailed structure of the shell-corrected potential profile. For example, in reactions 9 and 10,  $\delta V_B$ s are much higher than  $V_B^{\text{LD}}$ , and also, the corresponding  $k_s$  (0.75) is considerably larger than the usual value of 0.25. However, it is difficult to draw a unique connection among  $k_s$ ,  $\delta V_B$ , and  $V_B^{\text{LD}}$  as the latter two quantities change with the evaporation of each light particle. Also, the effect of  $\delta V_B$  in the free energy  $F$  depends on  $T$  as the shell effect disappears at higher  $T$  [26].

For  $V_B^{\text{LD}} \lesssim 3$  MeV, strong dissipation ( $k_s \geq 1$ ) is required to reach the experimental  $\nu_{\text{pre}}$ . For these reactions, the neutrons emitted outside the fission barrier contribute a moderate part of  $\nu_{\text{pre}}$ . Thus, the whole profile of  $\eta(c)$  [Eq. (1)] is crucial to decide the cumulative  $\nu_{\text{pre}}$ . We should point out that only a dynamical model with an explicit time evolution of the fission coordinate can identify neutron evaporation from different configurations. The distribution of evaporated neutrons from different configurations is demonstrated in Fig. 3 for a representative reaction from each category classified above. It shows that, irrespective of the mass region, the major contribution to  $\nu_{\text{pre}}$  comes from configurations around the ground state. Therefore,  $\nu_{\text{pre}}$  is sensitive to the static nuclear properties, such as the level density parameter mainly close to the ground state shape. Further, for fairly heavy systems [Fig. 3(c)], postbarrier dynamics is also important in deciding the final  $\nu_{\text{pre}}$ .

To validate the behavior of  $k_s$  extracted from  $\nu_{\text{pre}}$  data, we also calculated  $\langle E_K \rangle$  for the same values  $k_s$ . For reactions 10 and 14–17 in Table I, experimental  $\langle E_K \rangle$  are available for symmetric fission mode. We, therefore, considered these reactions and three other reactions closely resembling those in Table I, denoted here as A ( $^{16}\text{O} + ^{186}\text{W}$ ), B ( $^6\text{Li} + ^{232}\text{Th}$ ), and C ( $^{20}\text{Ne} + ^{232}\text{Th}$ ). Figure 4 compares the measured and calculated  $\langle E_K \rangle$  for different values of  $x_N$ . As expected, our model reproduces the experimental  $\langle E_K \rangle$  for actinides with  $x_N = 0.3$ . However, for lighter nuclei (A and reaction 10 in Table I), a lower  $x_N$  is required. It indicates a relatively elongated scission shape for lighter nuclei. Multidimensional Langevin dynamical calculations would be more conclusive in this regard. Interestingly, as presented in Fig. 4,  $\nu_{\text{pre}}$  is almost

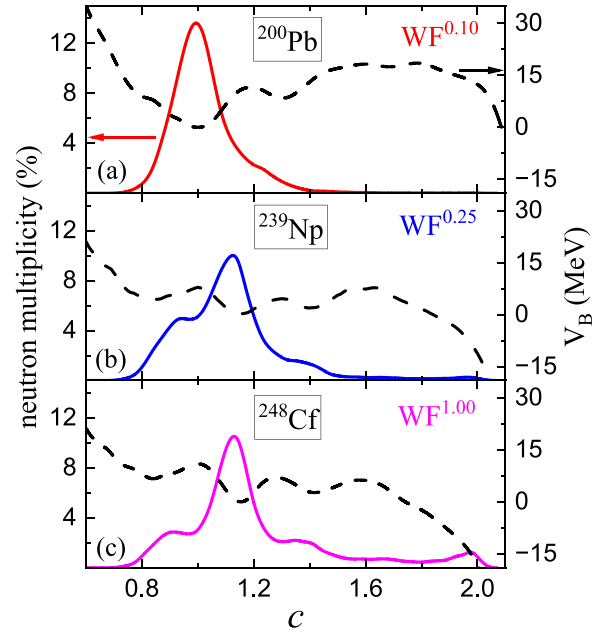


FIG. 3. Distributions of  $\nu_{\text{pre}}$  (solid lines and left axis) and shell-corrected potential energy  $V_B$  (dashed lines and right axis) along the compound nuclear deformation  $c$ . The CN and the used dissipation strengths are indicated in each panel following the same color scheme as in Fig. 2.

insensitive to  $x_N$  ( $\nu_{\text{pre}}$  changes by less than 3% in  $0.15 \leq x_N \leq 0.35$ ) as  $x_N$  only affects the neutron emission very close to the scission configuration. Therefore, we can simultaneously reproduce the measured  $\nu_{\text{pre}}$  and  $\langle E_K \rangle$  by varying  $k_s$  first and

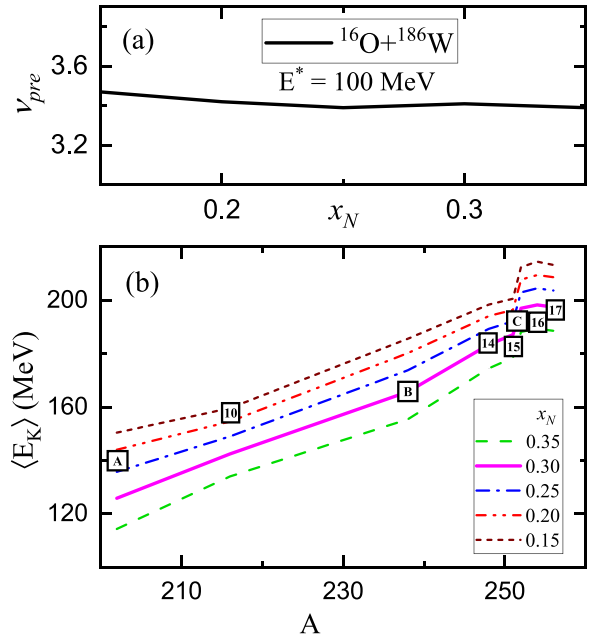


FIG. 4. (a) Calculated  $\nu_{\text{pre}}$  as a function of neck parameter  $x_N$  for the reaction and excitation energy as mentioned. (b) The experimental average TKEs (symbols as defined in the text) are compared with calculated average TKE (lines) for different  $x_N$  as mentioned.

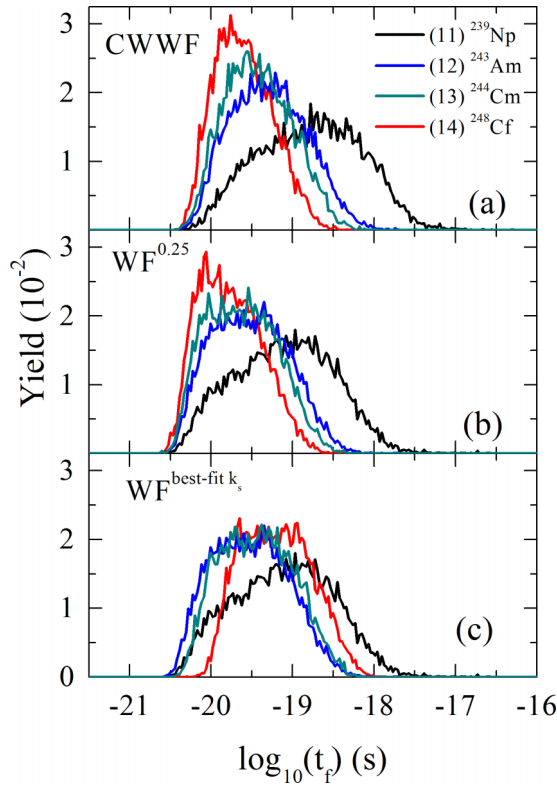


FIG. 5. Fission time ( $t_f$ ) distributions calculated with (a) CWWF, (b)  $WF^{0.25}$ , and (c) best-fit  $k_s$  for reactions as indicated in the top panel.

then  $x_N$ . Although  $x_N$  fine tunes  $\langle E_K \rangle$  by affecting  $V_{sc}$  and  $V_n$  in Eq. (4),  $\langle E_{sc} \rangle$  strongly depend on the amount of energy taken away by evaporated neutrons. Therefore,  $k_s$  plays a significant role in determining  $\langle E_K \rangle$ , and we have checked that the correct  $\langle E_K \rangle$  can only be achieved if we use the optimum  $k_s$  extracted in Fig. 2. It ensures that the obtained variations of  $k_s$  in the different mass regions are quite robust.

For a better understanding of the variation in  $k_s$ , we compared the fission time ( $t_f$ ) distributions in Fig. 5. Four representative reactions, 11–14, forming heavy compound nuclei  $^{239}\text{Np}$ ,  $^{243}\text{Am}$ ,  $^{244}\text{Cm}$ , and  $^{248}\text{Cf}$ , respectively, are considered for this purpose. A single energy point of 80 MeV is chosen for all four reactions, and only close-by masses are picked to minimize the perturbations due to the mass and energy dependencies in  $t_f$ . As shown in Fig. 5(a), the  $t_f$  distributions obtained with CWWF are quite distinct for different reactions: distributions become broader as the fission barrier increases. Also, the corresponding average fission times ( $\langle t_f \rangle$ ) for 11 and 14 differ by one order of magnitude as given in Table II. The mismatch in  $t_f$  distributions is somewhat reduced for  $WF^{0.25}$ , as shown in Fig. 5(b). The  $\langle t_f \rangle$  (Table II) also reduces, resulting in a lower  $\nu_{pre}$  for  $WF^{0.25}$  compared to CWWF. Interestingly, as shown in Fig. 5(c),  $t_f$  distributions and  $\langle t_f \rangle$ s as well (see Table II) become close for all the four reactions when the optimum  $k_s$ s are used. Therefore, we see that when the best fit  $k_s$  is used for actinide nuclei, similar  $V_B$  results in  $\langle t_f \rangle$  of the same order.

TABLE II.  $\langle t_f \rangle$  (in  $10^{-19}$  s) for different options of dissipation as given in Figs. 5 and 6.

Reaction from Table I	CWWF	$WF^{0.25}$	$WF^{\text{best-fit } k_s}$
1 $^{168}\text{Yb}$	134	92.9	147.7
2 $^{178}\text{W}$	428	265	259
3 $^{200}\text{Pb}$	435	281	185
4 $^{204}\text{Pb}$	376	251	179.5
5 $^{206}\text{Po}$	495	282	154.5
6 $^{210}\text{Po}$	212	125	125
7 $^{210}\text{Rn}$	153	69.2	101
8 $^{212}\text{Rn}$	135	24.7	120.3
9 $^{213}\text{Fr}$	97.3	42.1	111.5
10 $^{216}\text{Rn}$	13.0	1.6	9.97
11 $^{239}\text{Np}$	5.3	2.5	2.5
12 $^{243}\text{Am}$	0.9	0.5	0.5
13 $^{244}\text{Cm}$	0.6	0.38	0.6
14 $^{248}\text{Cf}$	0.3	0.26	1.0
15 $^{251}\text{Es}$	0.29	0.21	1.91
16 $^{254}\text{Fm}$	0.24	0.18	0.74
17 $^{256}\text{Fm}$	0.23	0.17	0.68

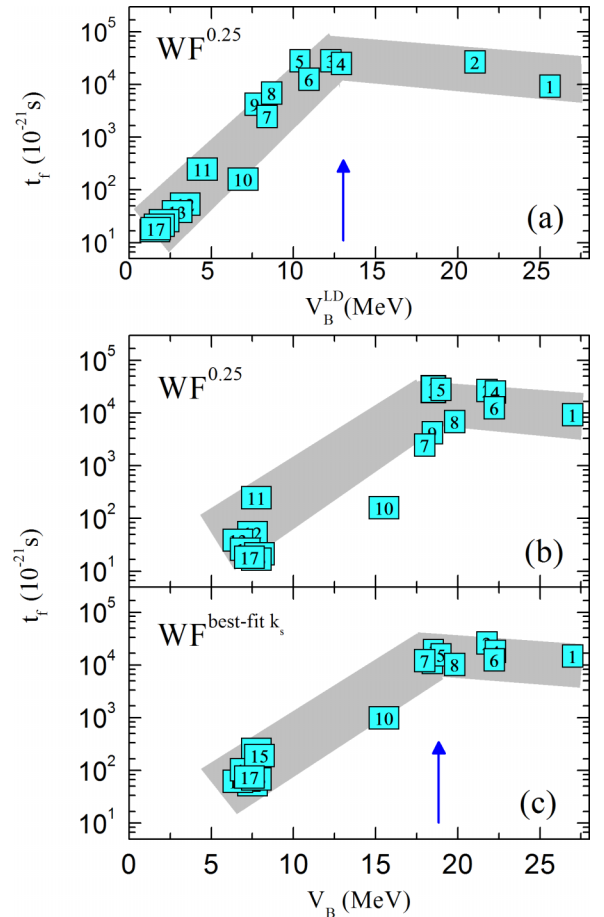


FIG. 6. Calculated  $\langle t_f \rangle$  as a function of fission barrier (a)  $V_B^{\text{LD}}$  and (b), (c)  $V_B$ . Calculations are done for different dissipation options, as indicated in each panel. Shaded bands are drawn to guide the eyes. Arrows indicate the values of  $V_B^{\text{LD}}$  and  $V_B$  where the nature of  $\langle t_f \rangle$  changes.

For further investigation, we calculated  $\langle t_f \rangle$  for all the reactions in Table I considering an energy window of  $80 \leq E^* \leq 85$  MeV. The values of  $\langle t_f \rangle$  are given in the Table II. Figure 6 shows the variation of  $\langle t_f \rangle$  as a function of  $V_B^{\text{LD}}$  and  $V_B$ . As illustrated,  $\langle t_f \rangle$  can be divided into two groups based on its variation with the fission barrier height: an almost exponentially increasing  $\langle t_f \rangle$  up to a certain barrier height and, then, a flat  $\langle t_f \rangle$  which mildly depends on the fission barrier. First, let us discuss the calculation with  $\text{WF}^{0.25}$ . Figure 6(a) shows that, for reactions with  $V_B^{\text{LD}} \gtrsim 13$  MeV,  $10^{-17} < \langle t_f \rangle < 10^{-16}$  s and is almost insensitive to the system considered. We found a similar trend for CWWF and for different energy ranges (not shown here). It complies with our preceding observation related to  $\nu_{\text{pre}}$ , i.e., the role of dynamics is minimal for large fission barriers.

$\log(\langle t_f \rangle)$  follows an almost linearly increasing trend with  $V_B^{\text{LD}}$  for lower barrier heights. Interestingly, it resembles the well-known analytical form for the fission probability,  $P_f \propto \exp(-V_B^{\text{LD}}/T)$  [57]. The correlation is partially removed [see Fig. 6(b)] when the total fission barrier  $V_B$  is considered instead of  $V_B^{\text{LD}}$ . However,  $\text{WF}^{0.25}$  does not reproduce the measured  $\nu_{\text{pre}}$ , and we rather expect  $\text{WF}^{\text{best-fit}k_s}$  to provide better results. This is evident in Fig. 6(c), where the correlation is again restored due to the local adjustment of  $k_s$  depending on the CN. Moreover, Fig. 6 shows two groups of  $\langle t_f \rangle$  along  $V_B$ :  $10^{-17} < \langle t_f \rangle < 10^{-16}$  s for  $V_B > 18$  MeV and  $\langle t_f \rangle \approx 10^{-19}$  s for  $V_B \approx 7$  MeV. Based on these findings, we can predict quantitative estimates of  $\langle t_f \rangle$  based on the magnitude of the calculated fission barrier. Future measurements of  $\nu_{\text{pre}}$  with compound nuclear fission barrier in the range of  $10 < V_B < 18$  MeV can establish our findings on a stronger footing.

#### IV. CONCLUSION

We performed a theoretical analysis of the measured precision neutron multiplicities for 17 reactions to understand the global characteristics of the shape-dependent one-body dissipation. These reactions form CN over a wide mass range of 168–256. The Langevin dynamical model for fission is used for the calculations with two different models of one-body dissipation, namely, wall-plus-window friction with  $k_s = 0.25$  and chaos-weighted wall-plus-window friction. We demonstrated that no single prescription of dissipation can explain the experimental  $\nu_{\text{pre}}$  for all the reactions. Further, the required dissipation strength is strongly correlated with the fission barrier height. This correlation is also reflected in the fission timescales, estimated by fitting the experimental  $\nu_{\text{pre}}$ . For weakly fissile systems with fission barrier  $V_B \gtrsim 18$  MeV, fission time is nearly insensitive to the compound nuclear properties. On the other hand, for nuclei with smaller fission barrier ( $\approx 6$ –7 MeV), fission probability tends to follow an exponential relation (similar to that conjectured by Kramers in a simplistic theoretical model) with the barrier height of the primary compound nucleus even in the presence of multichance fission events where different fission channels open up due to evaporation of light particles. This observation is helpful for a quantitative understanding of the stability of nuclei against fission.

#### ACKNOWLEDGMENTS

B.S. would like to thank Dr. B. K. Nayak for encouraging him to take up the work on fission dynamics using Langevin equations. The authors express their gratitude for the computing support received from the Super Computing Facility, BARC.

- 
- [1] P. Frobrich and I. I. Gontchar, *Phys. Rep.* **292**, 131 (1998).
  - [2] J. L. Rodríguez-Sánchez, J. Cugnon, J.-C. David, J. Hirtz, A. Kelić Heil, and I. Vidaña, *Phys. Rev. Lett.* **130**, 132501 (2023).
  - [3] D. Ramos *et al.*, *Phys. Rev. C* **107**, L021601 (2023).
  - [4] B. Li, D. Vretenar, Z. X. Ren, T. Nikšić, J. Zhao, P. W. Zhao, and J. Meng, *Phys. Rev. C* **107**, 014303 (2023).
  - [5] Y. Iwata and T. Nishikawa, *Phys. Rev. C* **105**, 044603 (2022).
  - [6] J. Zhao, T. Nikšić, and D. Vretenar, *Phys. Rev. C* **105**, 054604 (2022).
  - [7] C. Ishizuka, X. Zhang, K. Shimada, M. Usang, F. Ivanyuk, and S. Chiba, *Front. Phys.* **11**, 1111868 (2023).
  - [8] H. Eslamizadeh and H. Raanaei, *Phys. Rev. C* **107**, 054604 (2023).
  - [9] A. J. Sierk, *Phys. Rev. C* **96**, 034603 (2017).
  - [10] E. Vardaci, P. N. Nadtochy, A. Di Nitto, A. Brondi, G. La Rana, R. Moro, P. K. Rath, M. Ashaduzzaman, E. M. Kozulin, G. N. Knyazheva, I. M. Itkis, M. Cinausero, G. Prete, D. Fabris, G. Montagnoli, and N. Gelli, *Phys. Rev. C* **92**, 034610 (2015).
  - [11] P. N. Nadtochy, E. G. Ryabov, A. E. Gegechkori, Y. A. Anischenko, and G. D. Adeev, *Phys. Rev. C* **89**, 014616 (2014).
  - [12] K. Chakraborty, M. Senthil Kannan, J. Sadhukhan, and S. Mandal, *Phys. Lett. B* **843**, 138021 (2023).
  - [13] N. Wang and W. Ye, *Phys. Rev. C* **98**, 034614 (2018).
  - [14] J. Tian, N. Wang, and W. Ye, *Phys. Rev. C* **95**, 041601(R) (2017).
  - [15] M. Shareef, E. Prasad, A. Jhingan, N. Saneesh, S. Pal, A. M. Vinodkumar, K. S. Golda, M. Kumar, A. Shamlath, P. V. Laveen, A. C. Visakh, M. M. Hosamani, S. K. Duggi, P. S. Devi, G. N. Jyothi, A. Tejaswi, A. Chatterjee, and P. Sugathan, *Phys. Rev. C* **107**, 054619 (2023).
  - [16] R. Sandal *et al.*, *Phys. Rev. C* **87**, 014604 (2013).
  - [17] V. Singh, B. R. Behera, M. Kaur, A. Kumar, P. Sugathan, K. S. Golda, A. Jhingan, M. B. Chatterjee, R. K. Bhowmik, D. Siwal, S. Goyal, J. Sadhukhan, S. Pal, A. Saxena, S. Santra, and S. Kailas, *Phys. Rev. C* **87**, 064601 (2013).
  - [18] R. Kaur, M. Kaur, and S. Pal, *Phys. Rev. C* **106**, 024604 (2022).
  - [19] J. Gehlot, S. Nath, T. Banerjee, I. Mukul, R. Dubey, A. Shamlath, P. V. Laveen, M. Shareef, M. M. Shaikh, A. Jhingan, N. Madhavan, T. Rajbongshi, P. Jisha, and S. Pal, *Phys. Rev. C* **99**, 061601(R) (2019).
  - [20] K. Kapoor, N. Bansal, C. Sharma, S. Verma, K. Rani, R. Mahajan, B. R. Behera, K. P. Singh, A. Kumar, H. Singh, R. Dubey, N. Saneesh, M. Kumar, A. Yadav, A. Jhingan, P. Sugathan, B. K. Nayak, A. Saxena, H. P. Sharma, and S. K. Chamoli, *Phys. Rev. C* **100**, 014620 (2019).

- [21] Z. Matheson, S. A. Giuliani, W. Nazarewicz, J. Sadhukhan, and N. Schunck, *Phys. Rev. C* **99**, 041304(R) (2019).
- [22] J. Sadhukhan, W. Nazarewicz, and N. Schunck, *Phys. Rev. C* **93**, 011304(R) (2016).
- [23] D. J. Hinde, D. Hilscher, H. Rossner, B. Gebauer, M. Lehmann, and M. Wilpert, *Phys. Rev. C* **45**, 1229 (1992).
- [24] V. Weisskopf, *Phys. Rev.* **52**, 295 (1937).
- [25] J. P. Lestone, *Phys. Rev. Lett.* **70**, 2245 (1993).
- [26] M. T. Senthil Kannan, J. Sadhukhan, B. K. Agrawal, M. Balasubramaniam, and S. Pal, *Phys. Rev. C* **98**, 021601(R) (2018).
- [27] T. Banerjee, S. Nath, and S. Pal, *Phys. Lett. B* **776**, 163 (2018).
- [28] T. Banerjee, S. Nath, and S. Pal, *Phys. Rev. C* **99**, 024610 (2019).
- [29] J. Blocki, Y. Boneh, J. Nix, J. Randrup, M. Robel, A. Sierk, and W. Swiatecki, *Ann. Phys.* **113**, 330 (1978).
- [30] M. Brack, J. Damgaard, A. S. Jensen, H. C. Pauli, V. M. Strutinsky, and C. Y. Wong, *Rev. Mod. Phys.* **44**, 320 (1972).
- [31] S. Pal, G. Chaudhuri, and J. Sadhukhan, *Nucl. Phys. A* **808**, 1 (2008).
- [32] J. Sadhukhan and S. Pal, *Phys. Rev. C* **84**, 044610 (2011).
- [33] N. Kumar, S. Mohsina, J. Sadhukhan, and S. Verma, *Phys. Rev. C* **96**, 034614 (2017).
- [34] Y. Abe, S. Ayik, P. G. Reinhard, and E. Suraud, *Phys. Rep.* **275**, 49 (1996).
- [35] J. Sadhukhan and S. Pal, *Phys. Rev. C* **81**, 031602(R) (2010).
- [36] K. T. R. Davies, R. A. Managan, J. R. Nix, and A. J. Sierk, *Phys. Rev. C* **16**, 1890 (1977).
- [37] A. Bohr and B. Mottelson, *Nuclear Structure* (Benjamin, New York, 1969), Vol. 1.
- [38] A. J. Sierk, *Phys. Rev. C* **33**, 2039 (1986).
- [39] V. M. Strutinsky, *Nucl. Phys. A* **122**, 1 (1968).
- [40] F. Garcia, O. Rodriguez, J. Mesa, J. D. T. Arruda-Neto, V. P. Likhachev, E. Garrote, R. Capote, and F. Guzmán, *Comput. Phys. Commun.* **120**, 57 (1999).
- [41] P. Möller, A. J. Sierk, T. Ichikawa, A. Iwamoto, R. Bengtsson, H. Uhrenholt, and S. Åberg, *Phys. Rev. C* **79**, 064304 (2009).
- [42] A. V. Ignatyuk, M. G. Itkis, V. N. Okolovich, G. N. Smirenkin, and A. S. Tishin, *Yad. Fiz.* **21**, 1185 (1975).
- [43] W. Reisdorf, *Z. Phys. A* **300**, 227 (1981).
- [44] J. Newton, D. Hinde, R. Charity, J. Leigh, J. Bokhorst, A. Chatterjee, G. Foot, and S. Ogaza, *Nucl. Phys. A* **483**, 126 (1988).
- [45] N. K. Rai, A. Gandhi, A. Kumar, N. Saneesh, M. Kumar, G. Kaur, A. Parihari, D. Arora, K. S. Golda, A. Jhingan, P. Sugathan, T. K. Ghosh, J. Sadhukhan, B. K. Nayak, N. K. Deb, S. Biswas, and A. Chakraborty, *Phys. Rev. C* **100**, 014614 (2019).
- [46] K. Golda, A. Saxena, V. Mittal, K. Mahata, P. Sugathan, A. Jhingan, V. Singh, R. Sandal, S. Goyal, J. Gehlot, A. Dhal, B. Behera, R. Bhowmik, and S. Kailas, *Nucl. Phys. A* **913**, 157 (2013).
- [47] H. Singh, K. S. Golda, S. Pal, Ranjeet, R. Sandal, B. R. Behera, G. Singh, A. Jhingan, R. P. Singh, P. Sugathan, M. B. Chatterjee, S. K. Datta, A. Kumar, G. Viesti, and I. M. Govil, *Phys. Rev. C* **78**, 024609 (2008).
- [48] M. Strecker, R. Wien, P. Plischke, and W. Scobel, *Phys. Rev. C* **41**, 2172 (1990).
- [49] A. Saxena, A. Chatterjee, R. K. Choudhury, S. S. Kapoor, and D. M. Nadkarni, *Phys. Rev. C* **49**, 932 (1994).
- [50] K. Banerjee, T. K. Ghosh, S. Bhattacharya, C. Bhattacharya, S. Kundu, T. K. Rana, G. Mukherjee, J. K. Meena, J. Sadhukhan, S. Pal, P. Bhattacharya, K. S. Golda, P. Sugathan, and R. P. Singh, *Phys. Rev. C* **83**, 024605 (2011).
- [51] S. Björnholm, A. Bohr, and B. R. Mottelson, in *Proceedings of the International Conference on the Physics and Chemistry of Fission, Rochester, 1973* (IAEA, Vienna, 1974), Vol. 1.
- [52] S. Pal and T. Mukhopadhyay, *Phys. Rev. C* **54**, 1333 (1996).
- [53] G. Chaudhuri and S. Pal, *Phys. Rev. C* **65**, 054612 (2002).
- [54] A. V. Karpov, P. N. Nadtochy, D. V. Vanin, and G. D. Adeev, *Phys. Rev. C* **63**, 054610 (2001).
- [55] P. N. Nadtochy, G. D. Adeev, and A. V. Karpov, *Phys. Rev. C* **65**, 064615 (2002).
- [56] P. N. Nadtochy, E. G. Ryabov, A. E. Gegechkori, Y. A. Anischenko, and G. D. Adeev, *Phys. Rev. C* **85**, 064619 (2012).
- [57] H. Kramers, *Physica* **7**, 284 (1940).